

The Asymmetrical Eruption of a Quiescent Filament and Associated Halo CME

J. Yang · Y. Jiang · B. Yang · R. Zheng · D. Yang ·
J. Hong · H. Li · Y. Bi

Received: 8 October 2011 / Accepted: 15 April 2012 / Published online: 9 May 2012
© Springer Science+Business Media B.V. 2012

Abstract We will present detailed observations of the asymmetrical eruption of a large quiescent filament on 24 November 2002, which was followed by a two-ribbon flare, three coronal dimmings, endpoint brightenings, and a very fast halo-type coronal mass ejection (CME). Before the eruption, the filament lay along the main neutral line (MNL) underneath a single-arcade helmet streamer with a simple bipolar configuration. However, photospheric magnetic fields on both sides of the filament showed an asymmetrical distribution, and the filament and MNL were not located just at the center of the streamer base but were closer to the eastern leg of the streamer arcade. Therefore, instead of erupting along the streamer's symmetrical axis, the filament showed a nonradial and asymmetrical eruption. It lifted from the eastern flank of the streamer arcade to impact the western leg directly, leading to an asymmetrical CME that expanded westward; eventually the streamer was disrupted significantly. Accordingly, the opposite-polarity coronal dimmings at both sides of the filament forming in the eruption also showed an asymmetrical area distribution. We thus assume that the streamer arcade could guide the filament at the early eruption phase but failed to restrain it later. Consistent with previous results, these observations suggest that the global background magnetic field can impose additional action on the initial eruption of the filament and CME, as well as the dimming configuration.

Keywords Corona, activity · Coronal mass ejections, low coronal signatures · Magnetic fields, corona · Prominences, activity

J. Yang (✉) · Y. Jiang · B. Yang · R. Zheng · D. Yang · J. Hong · H. Li · Y. Bi
National Astronomical Observatories/Yunnan Astronomical Observatory,
Chinese Academy of Sciences, P.O. Box 110, Kunming 650011, China
e-mail: yjy@ynao.ac.cn

J. Yang
Key Laboratory for the Structure and Evolution of Celestial Objects, Chinese Academy of Sciences,
Kunming 650011, China

B. Yang · R. Zheng · D. Yang · J. Hong
Graduate School of Chinese Academy of Sciences, Beijing 100049, China

1. Introduction

Coronal mass ejections (CMEs) are striking manifestations of solar eruptions seen in the solar corona, which are often associated with flares, filament eruptions, coronal dimmings, and so on (Munro *et al.*, 1979; Poland *et al.*, 1981; Hudson and Cliver, 2001; Yashiro *et al.*, 2005). They bring coronal plasma as well as magnetic flux into interplanetary space. Therefore, they have significant impacts on space weather, and thus have been the subject of numerous studies. It is believed that the large-scale coronal structure is divided into open- and closed-field regions, represented by coronal holes and coronal helmet streamers, respectively (Hundhausen, 1977). As the interface of magnetically open and closed regions, helmet streamers are common structures in the Sun that are generally associated with CMEs (Illing and Hundhausen, 1986; Harrison *et al.*, 1990). Because CMEs must pass through the inner corona and encounter a different magnetic and plasma environment before moving into interplanetary space, helmet streamers can function as an agent of coronal reconfiguration and thus have a strong influence on the early propagation of CMEs (Low, 1994; Zhao and Webb, 2003; Liu and Hayashi, 2006; Shen *et al.*, 2011).

Many CMEs originated from the disruption of streamers (Illing and Hundhausen, 1986; Hundhausen, 1993; Low, 1996), and in some extreme cases, *i.e.*, streamer blowouts (Howard *et al.*, 1985), the pre-existing streamers were entirely destroyed. Previous observations showed that CMEs tended to be systematically offset in latitude from the centers of their source regions (Harrison, 1986; Kahler, Sheeley, and Liggett, 1989; Harrison *et al.*, 1990; Harrison, 1991; Kahler, 1992; Simnett, 2000; Gopalswamy *et al.*, 2003), and during the solar minimum CMEs can show a nonradial motion in the inner corona (St. Cyr *et al.*, 2000; Gopalswamy, Hanaoka, and Hudson, 2000; Plunkett *et al.*, 2001). More recently, it is recognized that CMEs that are laterally far offset from the source regions constitute a broad class called “over-and-out” CMEs which can be explained under the magnetic-arch-blowout scenario (Bemporad *et al.*, 2005; Moore and Sterling, 2007; Jiang *et al.*, 2009). Consistent with the previous suggestion of Webb *et al.* (1997) that the multiple-arcade complex is crucial for the understanding of many CME events, interaction or interplay between the arcades below a high-reaching streamer arcade is involved in such a scenario. Because some CMEs can also originate from symmetrical eruptions of concentric filaments in coronal streamers with simple bipolar field overlying single, straight neutral lines (Low, 1996; Gibson and Low, 1998), we wonder if a simple bipole-like helmet streamer configuration can result in the asymmetric eruption of filament and CME. If so, how does the background magnetic field work to shape the eruption in the inner corona?

On 24 November 2002, a full halo CME was observed to be associated with the eruption of a huge on-disk H α filament. The filament, located beneath a single-arcade helmet streamer and lying along its main polarity inversion line, erupted nonradially and asymmetrically, followed by a two-ribbon flare, spike-like endpoint brightenings, and three obvious coronal dimming regions. The streamer disrupted and disappeared completely after the CME, and potential field source surface (PFSS) modeling shows that the streamer had a simple bipolar magnetic field configuration. This allows us to investigate the cause of the asymmetrical filament eruption and the associated CME.

2. Observations

The observations used in the present study include the following:

- i) Full-disk $H\alpha$ line-center images from Big Bear Solar Observatory (BBSO), one station of the global $H\alpha$ network (Steinegger *et al.*, 2000). The image cadence is 1 min, and the pixel size is roughly $1''$.
- ii) Full-disk He I 10830 Å Doppler images from the Chromospheric Helium Imaging Photometer (CHIP), full-disk $H\alpha$ images from the Polarimeter for Inner Coronal Studies (PICS), and white-light observations of the low corona (1.08 to 2.85 solar radii) from the Mark IV K-coronameter (MK4) at Mauna Loa Solar Observatory (MLSO; MacQueen *et al.*, 1998). The CHIP data, having a 3-min cadence and a pixel size of $2.3''$, provide a measure of the line-of-sight velocity component over a range of $\pm 100 \text{ km s}^{-1}$ with an accuracy of approximately $\pm 5 \text{ km s}^{-1}$ (Gilbert *et al.*, 2001), and the PICS images have the same cadence as that of CHIP and a resolution of $2.9'' \text{ pixel}^{-1}$.
- iii) Full-disk EUV images with a pixel size of $2.6''$ from the Extreme ultraviolet Imaging Telescope (EIT; Delaboudinière *et al.*, 1995), full-disk line-of-sight magnetograms with a pixel size of $2''$ from the Michelson Doppler Imager (MDI; Scherrer *et al.*, 1995), and C2 white-light coronagraph data from the Large Angle and Spectrometric Coronagraphs (LASCO; Brueckner *et al.*, 1995) aboard the *Solar and Heliospheric Observatory* (SOHO). EIT images are taken in four spectral bands centered at Fe IX/X 171 Å, Fe XII 195 Å, Fe XV 284 Å, and He II 304 Å. For the present event, EIT 195 Å images were obtained continuously with a cadence of 12 min, while 171, 284, and 304 Å images were taken only once every 6 h.
- iv) Soft X-ray light curves observed by the *Geostationary Operational Environmental Satellite* (GOES) and CME height-time data available at the LASCO Web site.

3. Results

The eruptive filament, “F”, was located near the magnetic field inversion line between the two active regions AR10200 and AR10202. Its violent eruption started at about 19:13 UT, followed by an X-ray class C6.4 flare with the start, peak, and end times at around 20:14, 20:29, and 20:57 UT, respectively. Figure 1 shows the general appearance of the eruptive region. Before the eruption, F can be clearly seen in $H\alpha$ and EIT 195 Å (Figures 1(a) and 1(c)) along a neutral line dividing opposite-polarity photospheric magnetic fields (Figure 1(b)). F was centered at $N17^{\circ}E34^{\circ}$ with a position angle (PA) of about 60° and an angular extent of about 25° . As a reference direction, the radial direction of F, defined as a straight line connecting its centroid and the solar disk center, is shown by the white dashed lines in Figure 1. If F erupts symmetrically perpendicular to the solar surface, we will observe an eruption approximately along its radial direction (Loughhead, Wang, and Blows, 1983; McAllister *et al.*, 1996). This reference direction is also important for the stability of F, since its footpoints are subjected to the differential rotation. After the eruption, as a common characteristic of filament eruptions, post-eruptive coronal loops were observed to span the original F (Figure 1(d)). A remarkable characteristic of the event is that three coronal dimming regions, D1, D2, and D3, formed in the eruption. D1 and D2 were close to the southern end of F but lay on its different sides with opposite magnetic polarities, while D3 was a remote area to the northwest of F in a negative-polarity region. It is noteworthy that there was a dark lane (Levine, 1977), “DL”, adjacent to D3. To distinguish DL from D3, the boundary of DL determined from the 195 Å image at 17:35 UT before the eruption is shown as white dashed contours in Figures 1(b) and 1(d). We see that D3 was located close to the eastern border of DL.

The eruption process of F is shown in BBSO $H\alpha$, MLSO He I 10830 Å velocity, and EIT 195 Å direct images in Figure 2. In $H\alpha$ observations, F gradually disappeared after about

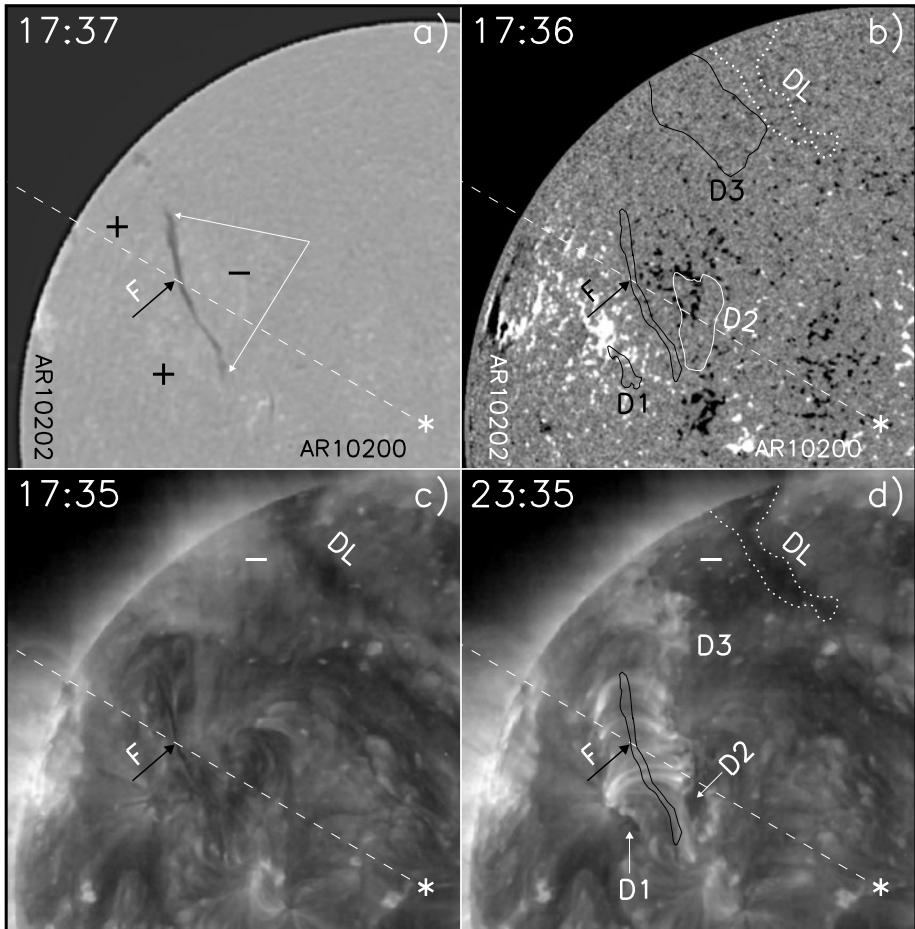


Figure 1 The general appearance of the eruptive region in MLSO $H\alpha$ image (a), MDI magnetogram (b), and EIT 195 Å images before (c) and after (d) the eruption. The black arrows indicate the centroid of the eruptive filament, “F”, the white arrows in (a) indicate F’s angular extent, and the dashed white lines indicate F’s radial direction. The plus/minus signs mark the corresponding positive/negative magnetic polarities on the photosphere. The outline of F from the $H\alpha$ image at 17:37 UT is superimposed on panels (b) and (d) as black contours. The outlines of three dimming regions, “D1”, “D2”, and “D3”, are shown as black or white solid contours in (b). The boundary of the dark lane, “DL”, determined from the 195 Å image at 17:35 UT before the eruption, is shown as white dashed contours in (b) and (d). The FOV is $1080'' \times 1100''$.

19:00 UT and then the flare occurred, with two ribbons located at both sides of the original F and showing an obvious increase in separation. The He 1 10830 Å velocity and EIT 195 Å observations clearly reveal another striking characteristic of the event: F’s eruption was not along its radial direction. F showed its first activity signature at about 18:35 UT followed by a slow rise. Then beginning at about 19:13 UT before the flare start, it quickly erupted nearly northwards. To trace the trajectory of the eruption, we need to set a fiducial point. Consistent with the definition of the radial direction and the northward eruption of F, we select its original centroid as the fiducial point, and the direction of F’s eruption is determined by the line connecting the top of the erupting F and the centroid. This is shown by the white

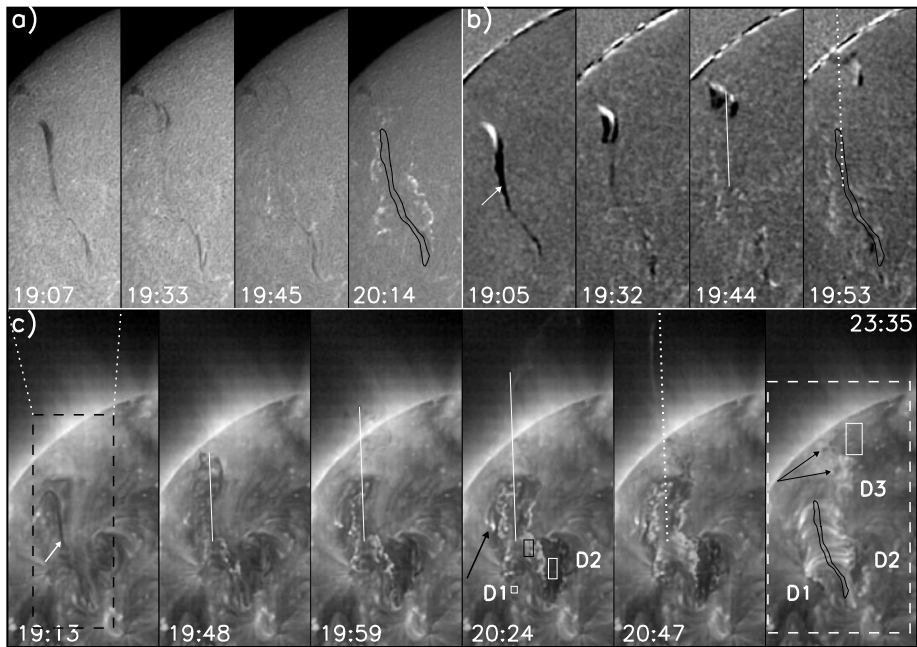


Figure 2 BBSO $H\alpha$ (a), MLSO He I 10830 Å Doppler velocity (b), and EIT 195 Å (c) images showing the eruption of F. The black arrow in the 195 Å image at 20:24 UT indicates the endpoint brightenings, and the black arrows in the 195 Å image at 23:35 UT indicate the remnant of F after its eruption. The white arrows in (b) and (c) indicate F's original centroid position, and the solid and dotted white lines indicate its direction of eruption. F's outlines are superimposed as black contours as in Figure 1. The solid boxes in (c) (in the images at 20:24 UT and 23:35 UT) mark the areas in which 195 Å light curves are measured and displayed in Figure 5. The FOV of images in (a) and (b) is $340'' \times 900''$, which is indicated by the dashed black box in (c), and the FOV of images in (c) is $640'' \times 1428''$.

solid and dashed lines in Figure 2. We see that F's eruption was nearly along a straight line tilted eastward at an angle of only about 2° from due north, *i.e.*, laterally offset to the north from F's radial direction by about 58° . By 20:47 UT when the erupting F was beyond the field of view (FOV) of EIT, it still kept a straight motion along the initial eruption path.

During the eruption, spike-shaped EUV brightenings occurred at the eastern side of the original F (indicated by the black arrow); Wang, Muglach, and Kliem (2009) called them "endpoint brightenings" because they could mark the far endpoints of the eruptive filament (see their Figure 9). It is clear that the two spreading flare ribbons were gradually connected by post-flare EUV loops, accompanied by the formation of the three dimmings. The initial appearances of D1 and D2 coincided with the start of the eruption of F, reached their maximum extent at about 20:24 UT, and then decreased in size as a result of expansion of the flare ribbons. However, it seems that D3 was ambiguous at first and then became more and more visible (see the EIT image at 23:25 UT). Although F disappeared in $H\alpha$ after the eruption, we note that its northern end still remained at the eastern boundary of D3 in EIT 195 Å (indicated by the black arrows in the 23:35 UT image). This is consistent with the previous result that a dark filament was more extended and better visible in EUV than in $H\alpha$ (Heinzl, Schmieder, and Tziotziou, 2001). Careful examination of EIT movies showed that the rest of F underwent two small jet-like eruptions at about 02:00 and 03:12 UT on

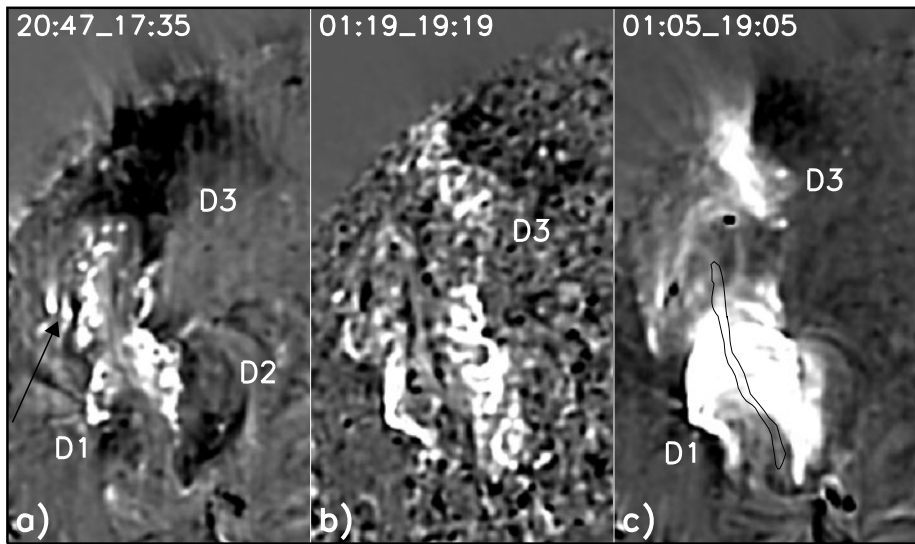


Figure 3 EIT 195 (a), 304 (b), and 284 Å (c) fixed-base difference images showing the coronal dimmings D1–D3. The black arrow indicates the endpoint brightenings, and F's outline is superimposed as a black contour as in Figure 1. The FOV is $640'' \times 1428''$.

25 November, respectively, indicating the continuation of the event on the first hours of the next day. Because these eruptions were close to D3, they might be associated with the expansion of coronal magnetic fields indicated by the formation of D3 (Jiang *et al.*, 2011; Yang *et al.*, 2012a). However, neither of the eruptions was related to a flare. No optical flare was reported by the Solar Geophysical Data online, and no GOES flare was registered around the time of the eruptions.

In Figure 3, we compare the difference between the pre-event and post-event images at 195, 304, and 284 Å. D1 and D2 are clearly discernible in the 195 Å image at 20:47 UT. D3 showed similar shapes in all of these wavelengths covering from 6×10^4 (304 Å) to 3×10^6 K (284 Å), suggesting that the dimming was probably due to a density loss instead of a temperature decrease of the coronal plasma (Thompson *et al.*, 1998). When we superimpose the outlines of D1 and D2 from the 195 Å image at 20:47 UT and of D3 from the 304 Å image at 01:19 UT of the next day onto the MDI magnetogram (Figure 1(b)), D2 and D3 occupy larger negative-polarity areas with low magnetic flux density, while the smaller positive-polarity area below D1 had high flux density. This property is similar to an example recently given by Yang *et al.* (2012b), and the asymmetry of dimmings in the opposite-polarity region is caused by the asymmetry in photospheric magnetic fields.

The following halo CME first appeared in the FOV of the LASCO C2 coronagraph at 19:54 UT, and later in the LASCO C3 at 20:42 UT as a bright loop front with a central PA of 340° . Figure 4 shows the structure and evolution of the CME, in which LASCO C2 fixed-base difference images are obtained by subtracting the 18:54 UT pre-event image (Figures 4(b1)–4(b7)) to display the erupting F and CME clearly. At first, we notice that the CME involved a disruption or a partial blowout of a pre-existing coronal helmet streamer (Howard *et al.*, 1985; Hundhausen, 1993). Before the CME, the streamer was clearly observed to include F and was centered at

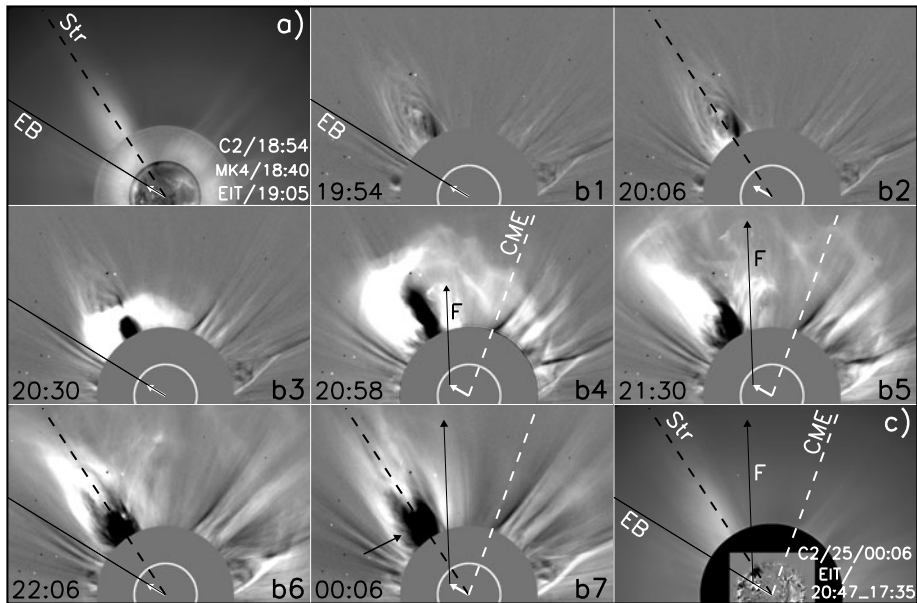
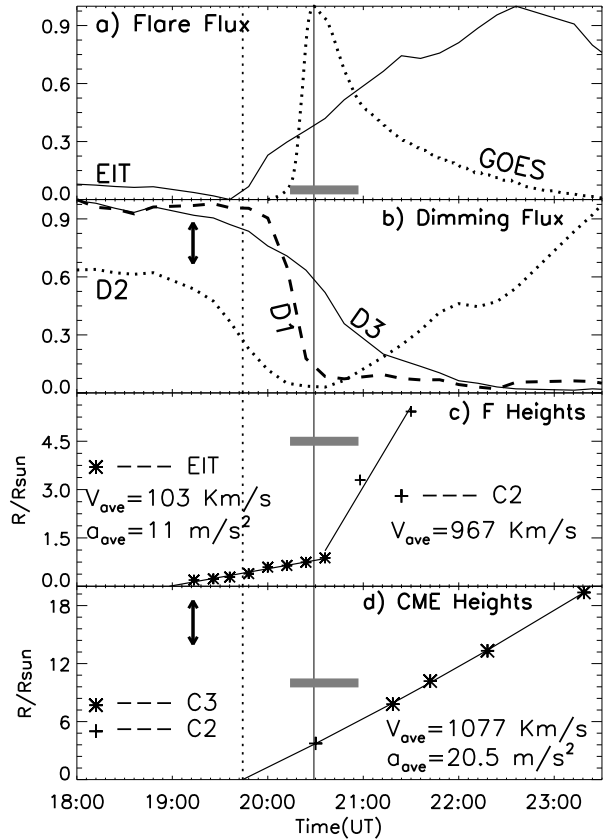


Figure 4 (a) Composite image of EIT 284 Å, MLSO MK4, and LASCO C2 direct images before the CME. (b1–b7) LASCO C2 fixed-base difference images. (c) Composite image of EIT 195 Å fixed-base difference and LASCO C2 direct images after the CME. The black solid (dashed) lines indicate the streamer’s eastern boundary EB (radial direction Str), respectively. The white (black) arrows indicate F’s original centroid position (direction of eruption), respectively. The dashed white lines indicate the direction of CME propagation.

about PA 33° (Figure 4(a)). Figure 4(a) also shows the radial direction (*i.e.*, the symmetrical axis of the streamer, “Str”), indicated by the dashed black lines and its eastern boundary, “EB”, indicated by the solid black lines. However, after the CME passage, the streamer exhibited a significant change in shape and brightness, leaving behind D3 just along its radial direction (Figure 4(c)). Clearly, the inner part of the streamer became dim by 00:06 UT of 25 November (indicated by the black arrow in Figure 4(b7)).

As mentioned above, EIT observations indicated the continuation of the event when the rest of F erupted on 25 November. Correspondingly, the LASCO movie from 25 November showed continued outflow along the streamer, and then the streamer blew out and disappeared completely after about 11:30 UT in the C2 FOV. In Figure 4, the final direction of CME propagation determined from its central PA is plotted as the dashed white lines, and the radial direction of the original F as the white arrows. Quite by chance, F’s radial direction almost coincided with EB, instead of Str. We see that the CME was first along Str (Figures 4(b1) and 4(b2)), and then expanded quickly to be a full halo CME after 20:30 UT. Although the brightest part of the CME front was nearly along Str, its expansion was mainly westward and its eastern edge was effectively limited by EB. Fortunately, the erupting F can be recognized easily behind the CME front in two images (Figures 4(b4) and 4(b5)); thus its direction of eruption, indicated by the black arrows, is identified with that from the He I 10830 Å Doppler velocity and EIT 195 Å observations. As a result, the eruptions of F and of the CME departed westward not only from F’s radial direction but also from the streamer’s symmetrical axis. Therefore, relative to the overlying streamer, they underwent asymmetrical eruptions.

Figure 5 Time profiles of GOES-10 1–8 Å soft X-ray flux (the dotted line in (a)) and the light curves of EIT 195 Å intensities in the flare and dimming areas marked by the solid boxes in Figure 2 (the solid line in (a) and the lines D1–D3 in (b)). The light curves are computed from the intensity integrated and normalized over these areas. (c) Filament heights along its eruption direction as a function of time, and the second-order (first-order) polynomial fitting to the measurements in the EIT (LASCO C2) FOV, respectively. (d) Heights of the CME front as a function of time, and the back extrapolation by the use of the second-order polynomial fitting. The vertical dotted line indicates the extrapolated CME onset time, while the vertical solid line shows the flare peak time. The heavy horizontal bars indicate the flare duration, and the arrows indicate the start time of the abrupt F eruption.



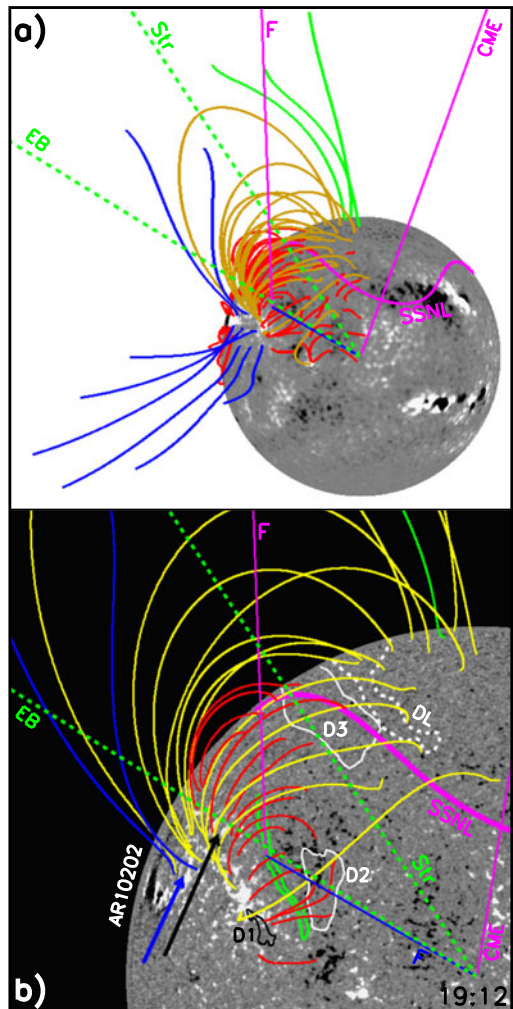
F's projected height measured from the original centroid position along its direction of eruption is derived from the EIT 195 Å and C2 white-light images, and is plotted in Figure 5(c). Figures 5(a) and 5(b) show the light curves of EIT 195 Å intensities in the three dimming regions and the flare region, to be compared with GOES-10 1–8 Å soft X-ray flux (Figure 5(a)) and the height-time (H–T) measurements of the CME front (Figure 5(d)). It is clear that the decreases or increases in the 195 Å intensities in the three dimming regions and the flare region took place nearly simultaneously with an abrupt eruption of F. Note that the intensity of D2 changed from decrease to increase due to the expansion of the flare ribbons. It seems that F's eruption had two distinct motion stages in the EIT and C2 FOVs: in the EIT FOV, F showed an average acceleration of 11.0 m s^{-2} and average speed of 103 km s^{-1} , which increased to 967 km s^{-1} . The application of the first-order and second-order polynomial fitting to the H–T points of the CME front in C2 FOV gives an average speed and acceleration of 1077 km s^{-1} and 20.5 m s^{-2} , respectively. In accordance with the result of Zhang *et al.* (2001), these parameters indicate that F possibly underwent a large acceleration at its early eruption phase, thus leading to the very fast CME. Furthermore, using the second-order polynomial fitting and extrapolating back the CME front from the H–T plots to the eruptive location yields an estimate of the CME onset time near 19:45 UT. This is close to the start times of the F eruption at 19:13 UT and the flare at 20:14 UT, implying a tight relationship between the F eruption and the CME.

4. Magnetic Configuration

An appropriate way to understand the asymmetrical nature of the eruption more deeply would be to place the event in the context of the global coronal field. The associated coronal magnetic field configuration is thus computed by using the Schrijver and De Rosa (2003) version of the PFSS model. The PFSS software package is available in SolarSoftWare based on synoptic magnetic maps from MDI with a 6 h time cadence, and the synoptic map at the time closest to the event studied here is used. In Figure 6, representative coronal magnetic field lines in association with the eruptive F and dimmings are shown, along with superposed outlines of the original F (green) and dimming regions D1–D3 (black and white), the directions of eruption of F and the CME (pink), the radial directions of F (blue) and the streamer (green), and the east boundary of the streamer (green).

Consistent with the coronagraph white-light observations shown in Figure 4 and the result of Wang, Muglach, and Kliem (2009), the event was associated with the bipolar

Figure 6 Overlay of full-disk (a) and zoomed-in (b) magnetograms with the extrapolated field lines. Closed-field lines are coded in yellow if they extend beyond 1.2 solar radii, and coded in red otherwise. Open-field lines directed inward and outward are coded in green and blue, respectively, and the pink curves are the computed source surface neutral line (SSNL). The dashed green lines indicate the streamer's eastern boundary (EB) and radial direction (Str), the blue lines indicate F's radial direction, and the pink lines indicate the eruption directions of F and the CME. The outlines of the original F and the three dimming regions are superimposed as green, white, and black contours. The black arrow indicates the EUV endpoint brightenings, and the blue arrow indicates the footpoints of outward open fields in the neighborhood of AR10202.



single-arcade helmet streamer belt (Zhao and Webb, 2003), as modeled by the PFSS. First, we see that bipolar closed-field regions, indicated by yellow and red field lines, are sandwiched between opposite-polarity open-field regions represented by blue and green field lines. Second, the helmet streamer belt reaches the source surface at 2.5 solar radii where its cusp defines the base of the heliospheric current sheet (HCS) (Smith, 2001), and the radial field is set to zero there. This is identified with the computed source surface neutral line (SSNL), which is projected down onto the photospheric magnetogram and plotted as the pink curve. Finally, the overall closed fields had a simple bipole-like configuration; thus only one main neutral line (MNL) existed below the streamer, and undoubtedly F lay along the single MNL in the photosphere. Such a simple bipole-like configuration suggests that a multipolar geometry is not a necessary condition for an eruption (Wang, Muglach, and Kliem, 2009). However, we see that F lay in the eastern outer flank rather than at the center of the streamer base. This situation is somewhat similar to that of the over-and-out CMEs (Harrison, 1986; Bemporad *et al.*, 2005; Moore and Sterling, 2007; Jiang *et al.*, 2009; Yang *et al.*, 2011). A difference is that the reported over-and-out CME events involved complex, multiple-arcade helmet streamers, and the eruptive filaments or flares lay below one of the lower arcades instead of along the MNLs of the streamers. In our case, F was along the single MNL but clearly offset from Str (namely, from the SSNL's projection), indicating that the high field lines of the streamer were symmetrical with respect to Str while its low field lines were not. The condition of the photospheric magnetic field around F was such that the positive-polarity region to the east of F was compact, whereas the negative-polarity region to its northwest was dispersed and covered D3 and DL. This causes MNL and F to be shifted from the geometrical center of the streamer. Similar to the situation described by the magnetic-arch-blowout scenario (Moore and Sterling, 2007), it is very likely that, at the initial eruption phase, F interacted with a leg of the adjacent, overlying field that was strong enough to laterally deflect the F eruption from moving radially outward, resulting in the following asymmetrical eruptions of F and the CME. It is also found that the open field lines (blue in Figure 6) are directed outward in the neighborhood of AR10202 (see the blue arrow), probably indicating that a flux emergence in AR10202 is the source of the open magnetic flux (Wang and Sheeley, 2002; Liu and Hayashi, 2006) and could be related to the trigger of the F eruption.

D1 and D2 were located close to the opposite-polarity footpoints of the lower field lines around F's southern end; therefore, they were probably produced by the stretching or opening of these field lines. On the other hand, the remote D3 was located on the western footpoints of the higher field lines, whereas its opposite-polarity counterpart corresponded to the endpoint brightenings (indicated by the black arrow in Figure 6). Because F was closer to the eastern footpoints of the higher field lines than the western ones, one reason for this phenomenon might be that any eastern dimmings would have been masked by the flare ribbons or by the rapid endpoint brightenings. Another cause may be the asymmetrical F eruption that was not along the symmetric axis of the low coronal arches but impacted to its western part directly. Thus it is plausible that the western part of the field lines underwent more stretching and the formation of western dimmings was easier.

Consistent with previous observations (Cremades and Bothmer, 2004; Liu, 2007; Gui *et al.*, 2011), our event suggests that the global background magnetic field might control the dimming configuration and dynamic process in the inner corona during the associated filament and CME eruptions. Unlike the cases in which the axis of a CME tends to locally align itself with the HCS (Mulligan *et al.*, 2001; Yurchyshyn, 2008), the F eruption in our case was so violent that the streamer was disrupted and resulted in the very fast halo CME. The erupting F first approached the SSNL but then maintained its initial eruption direction.

As a result, the streamer changed significantly, and the final CME did not run along the streamer's axis but expanded quickly to the west.

5. Discussion

In this paper, we have investigated the asymmetrical eruption of a large quiescent filament followed by a two-ribbon flare and a very fast halo CME. Along the single main neutral line of the bipolar single-arcade helmet streamer belt that was offset eastward from the center of the streamer base, the filament, which was embedded in an asymmetrical bipole-like magnetic field topology and adjacent to open magnetic fields, erupted, probably triggered by the flux emergence in the neighborhood. The flux emergence is expected to significantly change the magnetic configuration around the filament and thus might play an important role in triggering its eruption (Feynman and Martin, 1995; Jiang, Shen, and Wang, 2007). The initial filament eruption was from the eastern outer flank of the streamer base and thus could be guided by the streamer arcade at first, but its later eruption was not along the streamer. Instead, the filament struck the western leg of the streamer arcade, the following CME showed obvious westward expansion, and then the streamer was disrupted. The asymmetry of the eruption and the dimming configuration were probably associated with the asymmetrical magnetic field topology, consisting of the asymmetrical magnetic field settings at the streamer base in the photosphere. Therefore, the final outcome of the eruption was determined not only by the initial nature of the filament eruption but also by the surrounding magnetic field (Liu, 2007; Zuccarello *et al.*, 2012).

Acknowledgements We would like to thank an anonymous referee for a constructive and useful review of the paper. We are also grateful to the staff at BBSO for making quality observations. MLSO's data are provided by the High Altitude Observatory of the National Center for Atmospheric Research, which is sponsored by the National Science Foundation. We thank the GOES team and the SOHO/EIT, LASCO, and MDI teams for data support. This work is supported by the 973 Program (2011CB811403) and by the Natural Science Foundation of China under grants 10973038 and 11173058.

References

- Bemporad, A., Sterling, A.C., Moore, R.L., Poletto, G.: 2005, *Astrophys. J. Lett.* **635**, L189.
- Brueckner, G.E., Howard, R.A., Koomen, M.J., Korendyke, C.M., Michels, D.J., Moses, J.D., *et al.*: 1995, *Solar Phys.* **162**, 357.
- Cremades, H., Bothmer, V.: 2004, *Astron. Astrophys.* **422**, 307.
- Delaboudinière, J.-P., Artzner, G.E., Brunaud, J., Gabriel, A.H., Hochedez, J.F., Millier, F., *et al.*: 1995, *Solar Phys.* **162**, 291.
- Feynman, J., Martin, S.F.: 1995, *J. Geophys. Res.* **100**, 3355.
- Gibson, S.E., Low, B.C.: 1998, *Astrophys. J.* **493**, 460.
- Gilbert, H.R., Holzer, T.E., Low, B.C., Burkeoile, J.T.: 2001, *Astrophys. J.* **549**, 1221.
- Gopalswamy, N., Hanaoka, Y., Hudson, H.S.: 2000, *Adv. Space Res.* **25**, 1851.
- Gopalswamy, N., Shimojo, M., Lu, W., Yashiro, S., Shibasaki, K., Howard, R.A.: 2003, *Astrophys. J.* **586**, 562.
- Gui, B., Shen, C., Wang, Y., Ye, P., Liu, J., Wang, S., *et al.*: 2011, *Solar Phys.* **271**, 111.
- Harrison, R.A.: 1986, *Astron. Astrophys.* **162**, 283.
- Harrison, R.A., Hildner, E., Hundhausen, A.J., Sime, D.G., Simnett, G.M.: 1990, *J. Geophys. Res.* **95**, 917.
- Harrison, R.A.: 1991, *Adv. Space Res.* **11**, 25.
- Heinzel, P., Schmieder, B., Tziotziou, K.: 2001, *Astrophys. J.* **561**, L223.
- Howard, R.A., Sheeley, N.R. Jr., Michels, D.J., Koomen, M.J.: 1985, *J. Geophys. Res.* **90**, 8173.
- Hudson, H.S., Cliver, E.W.: 2001, *J. Geophys. Res.* **106**, 199.

- Hundhausen, A.J.: 1977, In: Zirker, J.B. (ed.) *Coronal Holes and High Speed Wind Streams*, Colorado Assoc. Univ. Press, Boulder, 225.
- Hundhausen, A.J.: 1993, *J. Geophys. Res.* **98**, 13177.
- Illing, R.M.E., Hundhausen, A.J.: 1986, *J. Geophys. Res.* **91**, 10951.
- Jiang, Y., Shen, Y., Wang, J.: 2007, *Chin. J. Astron. Astrophys.* **7**, 129.
- Jiang, Y., Yang, J., Hong, J., Bi, Y., Zheng, R.: 2011, *Astrophys. J.* **738**, 179.
- Jiang, Y., Yang, J., Zheng, R., Bi, Y., Yang, X.: 2009, *Astrophys. J.* **693**, 1851.
- Kahler, S.W., Sheeley, N.R. Jr., Liggett, M.: 1989, *Astrophys. J.* **344**, 1026.
- Kahler, S.W.: 1992, *Annu. Rev. Astron. Astrophys.* **30**, 113.
- Levine, R.H.: 1977, *Astrophys. J.* **218**, 291.
- Liu, Y., Hayashi, K.: 2006, *Astrophys. J.* **640**, 1135.
- Liu, Y.: 2007, *Astrophys. J. Lett.* **654**, L171.
- Low, B.C.: 1994, *Plasma Phys.* **1**, 1684.
- Low, B.C.: 1996, *Solar Phys.* **167**, 217.
- Loughhead, R.E., Wang, J.-L., Blows, G.: 1983, *Astrophys. J.* **274**, 883.
- MacQueen, R.M., Blankner, J.G., Elmore, D.F., Lecinski, A.R., White, O.R.: 1998, *Solar Phys.* **182**, 97.
- McAllister, A.H., Kurokawa, H., Shibata, K., Nitta, N.: 1996, *Solar Phys.* **169**, 123.
- Moore, R.L., Sterling, A.C.: 2007, *Astrophys. J.* **661**, 543.
- Mulligan, T., Russell, C.T., Elliott, D., Gosling, J.T., Luhmann, J.G.: 2001, *Geophys. Res. Lett.* **28**, 891.
- Munro, R.H., Gosling, J.T., Hildner, E., Macqueen, R.M., Poland, A.I., Ross, C.L.: 1979, *Solar Phys.* **61**, 201.
- Plunkett, S.P., Thompson, B.J., St. Cyr, O.C., Howard, R.A.: 2001, *J. Atmos. Solar-Terr. Phys.* **63**, 389.
- Poland, A.I., Howard, R.A., Koomen, M.J., Michels, D.J., Sheeley, N.R. Jr.: 1981, *Solar Phys.* **69**, 169.
- Scherrer, P.H., Bogart, R.S., Bush, R.I., Hoeksema, J.T., Kosovichev, A.G., Schou, J., *et al.*: 1995, *Solar Phys.* **162**, 129.
- Schrijver, C.J., De Rosa, M.L.: 2003, *Solar Phys.* **212**, 165.
- Shen, C., Wang, Y., Gui, B., Ye, P., Wang, S.: 2011, *Solar Phys.* **269**, 389.
- Simnett, G.M.: 2000, *J. Atmos. Solar-Terr. Phys.* **62**, 1479.
- Smith, E.J.: 2001, *J. Geophys. Res.* **106**, 15819.
- St. Cyr, O.C., Plunkett, S.P., Michels, D.J., Paswaters, S.E., Koomen, M.J., Simnett, G.M., *et al.*: 2000, *J. Geophys. Res.* **105**, 18169.
- Steinberger, M., Denker, C., Goode, P.R., Marquette, W.H., Varsik, J., Wang, H., *et al.*: 2000, In: Wilson, A. (ed.) *The Solar Cycle and Terrestrial Climate, ESA SP-463*, 617.
- Thompson, B.J., Plunkett, S.P., Gurman, J.B., Newmark, J.S., St. Cyr, O.C., Michels, D.J.: 1998, *J. Geophys. Res.* **25**, 2465.
- Wang, Y.-M., Muglach, K., Kliem, B.: 2009, *Astrophys. J.* **699**, 133.
- Wang, Y.-M., Sheeley, N.R. Jr.: 2002, *J. Geophys. Res.* **107**, 1302.
- Webb, D.F., Kahler, S.W., McIntosh, P.S., Klimchuck, J.A.: 1997, *J. Geophys. Res.* **102**, 24161.
- Yang, J., Jiang, Y., Zheng, R., Hong, J.C., Bi, Y., Yang, L.H.: 2011, *Solar Phys.* **270**, 551.
- Yang, J., Jiang, Y., Zheng, R., Bi, Y., Hong, J., Yang, B.: 2012a, *Astrophys. J.* **745**, 9.
- Yang, J., Jiang, Y., Bi, Y., Li, H., Hong, J., Yang, D., Zheng, R., Yang, B.: 2012b, *Astrophys. J.* **749**, 12.
- Yashiro, S., Gopalswamy, N., Akiyama, S., Michalek, G., Howard, R.A.: 2005, *J. Geophys. Res.* **110**, A12S05.
- Yurchyshyn, V.: 2008, *Astrophys. J. Lett.* **675**, L52.
- Zhang, J., Dere, K.P., Howard, R.A., Kundu, M.R., White, S.M.: 2001, *Astrophys. J.* **559**, 452.
- Zhao, X.P., Webb, D.F.: 2003, *J. Geophys. Res.* **108**, 1234.
- Zuccarello, F.P., Bemporad, A., Jacobs, C., Mierla, M., Poedts, S., Zuccarello, F.: 2012, *Astrophys. J.* **744**, 66.